Journal of New Results in Engineering and Natural Science, No:21 (2024) 30-46
https://dergipark.org.tr/tr/pub/jrens

Received: 04.12.2024
Accepted: 20.12.2024

Design of Double-Stator Axial Flux Permanent Magnet Synchronous Motor

Sümeyye SARIDAĞ[1*], Mustafa EKER[1]

[1], *Electrical and Electronics Engineering, Institute of Graduate Studies, Tokat Gaziosmanpasa University, Tokat, TURKEY*

Abstract

In this study, the design of a Double-Stator Single-Rotor Axial Flux Permanent Magnet Synchronous Motor (DS-AFSM) is discussed. The motor design is carried out using an analytical approach, followed by a 3D solid model of the motor. The performance of the motor is investigated in detail using the Finite Element Method (FEM), and based on the preliminary results, optimization studies are carried out to improve the torque ripple value. In the optimization process, parameters such as the embrace, the inner diameter, and the outer diameter of the magnet were optimized using the Multi-Objective Genetic Algorithm (MOGA) method. In this way, a 67.42% decrease in the torque ripple value and a 5.15% increase in the average torque values were achieved, and the targeted values were obtained. Finally, the load characteristic of the designed motor is extracted with FEM, and the performance of the motor under real operating conditions is analyzed. At the rated load value of the motor, the efficiency is 92.41%, and the stator current RMS average value is 5.61 A. This study aims to contribute to the design and optimization processes of the Axial Flux Motor (AFM).
.

Keywords: AFM, FEM, MOGA.

Çift Statorlu Eksenel Akılı Sürekli Mıknatıslı Senkron Motor Tasarımı

Sümeyye SARIDAĞ, Mustafa EKER

Özet

Bu çalışmada, Çift Statorlu Tek Rotorlu Eksenel Akılı Sürekli Mıknatıslı Senkron Motor tasarımı ele alınmıştır. Motor tasarımı analitik bir yaklaşımla gerçekleştirilmiş, ardından motorun 3B katı modeli oluşturulmuştur. Motorun performansı, Sonlu Elemanlar Yöntemi kullanılarak detaylı bir şekilde incelenmiş ve elde edilen ilk sonuçlar doğrultusunda, tork ripple değerinin iyileştirilmesine yönelik optimizasyon çalışmaları yapılmıştır. Optimizasyon sürecinde, MOGA (Çok Amaçlı Genetik Algoritma) yöntemi kullanılarak mıknatısın embrace, iç çapı ve dış çapı gibi parametreler optimize edilmiştir. Bu sayede, tork ripple değerinde %67.42 düşüş ve ortalama tork değerlerinde %5.15'lik bir artış sağlanmış ve hedeflenen değerler elde edilmiştir. Son olarak, tasarlanan motorun yük karakteristiği Sonlu Elemanlar Yöntemi ile çıkarılarak, motorun gerçek çalışma koşullarındaki performansı analiz edilmiştir. Motor nominal yük değerinde verim %92.41 ve stator akım rms ortalama değeri 5.61A olarak elde edilmiştir. Bu çalışma, eksenel akılı motor tasarımı ve optimizasyon süreçlerine katkı sağlamayı amaçlamaktadır.
.

Keywords: Eksenel Akılı Motor, SEY, MOGA.

[*]*Corresponding Author*, e- mail: sumeyye.saridag1822@gop.edu.tr

1. Introduction

Since the invention of the first electric motor, electric motor technology has undergone a significant evolution through many different design stages. Technological advances and increasing energy demand require motors to be more efficient, economical, durable, and user-friendly. Today, electric motors are optimized in terms of key parameters such as efficiency, power, speed, and size. This optimization process is accelerated by the determination of design parameters, analytical calculations, the use of modeling techniques, and the integration of computer-aided simulation programs. While new motor designs provide improvements to existing motors, increased performance allows for more efficient and sustainable options to come to the forefront in production processes [1], [2], [3].

Tausif et al. compared the torque density, power factor, and efficiency of different rotor and stator configurations in Axial Flux Permanent Magnet (AFPM) machines using the Finite Element Method (FEM). They concluded that double-sided structures achieve higher torque density than single-sided structures. They also investigated the torque-speed ranges of double-stator single-rotor machines with internal and surface magnet configurations. Comparison of double-stator single-rotor machines with internal and surface magnet configurations emphasized that internal magnets increase the saliency and improve the torque-speed range [4]. Mahmoudi et al. optimized motors with different numbers of slots to obtain maximum power density using a Genetic Algorithm (GA) based design equation and used FEM to perform electromagnetic field analysis on the resulting designs. They have studied in detail methods such as redesigning the winding structure and skewing the permanent magnets to achieve a more sinusoidal back EMF waveform and lower cogging torque. They tested the best configuration in production and obtained successful simulation and test results [5]. Pamuk created a mathematical model for the determination of critical values depending on five optimization variables for the optimal design of AFPM. The author calculated the losses of the motor designed by combining the optimization performed by the author using GA with the FEM [6].

AFPMs have a history going back nearly two hundred years, with the foundations of these motors dating back to the discoveries made by Michael Faraday in 1831. Although Faraday patented the first Axial Flux Motors (AFM), the popularity of these motors was significantly contributed to the advancement of this motor technology by the discovery of rare earth magnets [7], [8]. Magnet-containing motors use magnets rather than rotor windings to provide the field flux, in contrast to traditional rotor-wound motors. This design improves the motor's efficiency while reducing energy losses. In these motors, the absence of brushes and collectors in the rotor eliminates mechanical friction and wear problems that are frequently encountered in brush motors, reducing maintenance and repair costs[9]. In addition, the absence of copper losses improves the electrical efficiency of the motor and reduces overall energy consumption [10]. Furthermore, the absence of magnetizing current in the stator of the motor allows the power coefficient to be increased. This significantly improves the performance of the motor, because the magnetizing current is a factor that directly affects the operating efficiency of the motor [11], [12].

In AFMs, spreading the magnetic field parallel to the axis of rotation shortens the magnetic path and makes the motor more compact[13]. This design reduces the size of the motor while at the same time ensuring high power density and efficient torque production. This compact structure makes it possible for the motors to be lighter and have higher torque-to-weight ratios. Thus, AFPM motors offer a more efficient and advantageous alternative to conventional motors, especially in applications where high performance and low energy dissipation requirements exist [14], [15].

Double-Stator Single-Rotor Axial Flux Synchronous Motors (DS-AFPMs) are machines specifically developed to meet the requirements of high power density, efficiency, and torque generation. These

motors generate more magnetic field with the two-layer structure of the stator, which allows the motor to operate with higher performance and efficiency. The double-stator structure helps the motor to run more stably under load, while at the same time providing less heating and low energy loss. The axial flux structure provides a linear orientation of the magnetic field between the rotor and stator, allowing for high torque production. Such motors are mainly used in electric vehicles, renewable energy systems, and industrial applications. Advantages include high efficiency, compact design, and low-cost production, while disadvantages include complexity and high engineering requirements. Double-stator motors are ideal for industries looking for efficient and powerful solutions that increase power density with a smaller space footprint [14], [15], [16].

In this study, considering the advantages of a double-stator single-rotor structure, such as high torque, vibration, and a balanced structure, a DS-AFPM was designed by using the stator dimensions of a mass-produced single-sided AFM. It is aimed to create a motor structure operating with high efficiency. NN-type rotor structure was preferred in the design, and electromagnetic results of this structure were analyzed. In the results obtained, improvement studies were carried out on the average torque and torque oscillation values. The Multi-Objective Genetic Algorithm (MOGA) method was used to increase the average torque and reduce the torque oscillation. In this process, the magnet embrace, the magnet inner diameter, and the magnet outer diameter dimensions were optimized. After the mathematical modeling of the design process, analytical design and 3D solid modeling were analyzed with FEM.

This study consists of 5 main chapters. The first section is the INTRODUCTION, where general information and the purpose of the study are given. The second chapter is Material and Method, where the structure of the DS-AFSM, analytical calculations, as well as the MOGA optimization method are given. Chapter 3 is Design and Result, where the design and optimization processes are described and the results obtained are presented. Section 4 is the RESULT section, where the electromagnetic results obtained by FEM of the 3D solid model are given. The last chapter is the CONCLUSION chapter, where the results of the study are evaluated.

2. Material and Method

2.1. DS-AFPM

The DS-AFSM is mainly composed of three main components: double-stator, single-rotor, and permanent magnets. In the structural design of this motor, both stators are located around the rotor, and each is responsible for magnetic field generation. The stators are equipped with permanent magnets that direct the magnetic field, usually in a cylindrical structure. The rotor interacts with the magnetic field located in the axial direction and produces rotational motion [14]. The double-stator design optimizes the overall efficiency while increasing the torque production of the motor. Furthermore, the spreading of the magnetic flux in the axial direction allows the motor to be more compact and have high-power density, which offers a significant advantage, especially for electric vehicles and industrial applications. Figure 1 shows the visuals of AFM and Radial Flux Motor (RFM) structures. AFMs transmit magnetic flux in a direction parallel to the motor axis, while RFMs conduct magnetic flux in a direction perpendicular to the motor axis. In AFMs, the magnetic flux generally travels shorter paths, resulting in a more efficient and powerful magnetic field. In RFMs, on the other hand, the magnetic flux travels longer paths, leading to efficiency losses and a larger motor structure.

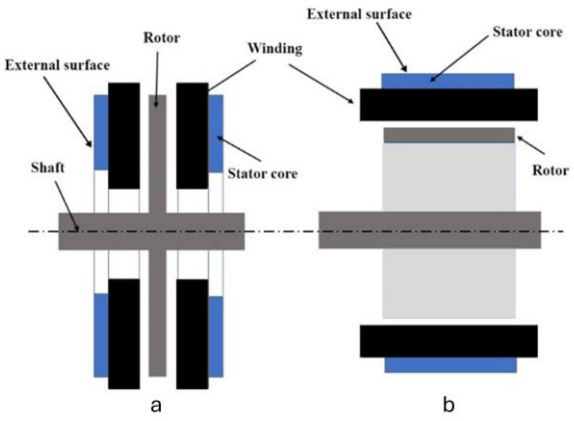

Figure 1. Axial Flux (a) and Radial Flux (b) motor representations [17]

AFMs are a type of motor in which the magnetic field is directed parallel to the axis of the motor and are generally preferred to provide high torque and efficiency. These motors can be divided into different categories according to the number of stators and rotors. Stator and rotor numbers directly affect the structural characteristics and operating performance of the motor, creating variations in important parameters such as power output, efficiency, and torque generation. Thus, in the design of AFMs, these numbers play a decisive role in optimizing the motor for the application area. Figure 2 shows the combinations of AFMs according to the stator and rotor numbers.

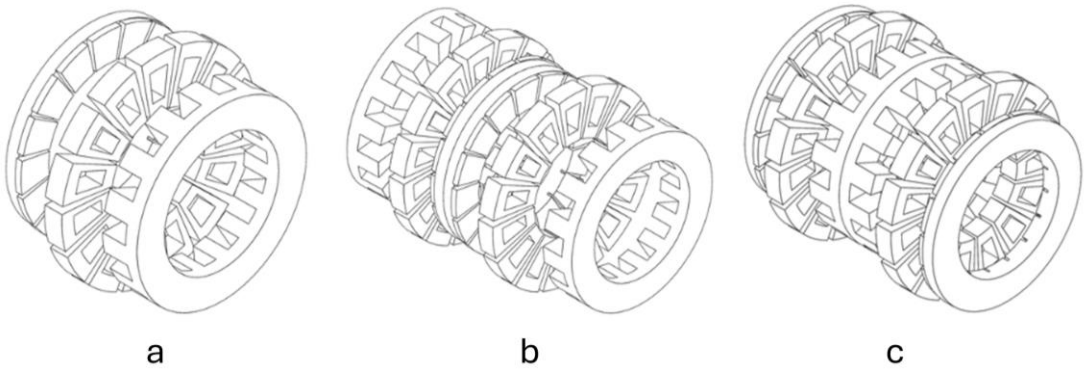

Figure 2. Prevalent AFPM Motor Topologies (a- Single-Stator Single-Rotor, b- Double-Stator Single-Rotor, c- Single-Stator Double-Rotor) [18]

Single-Stator Single-Rotor (SSSR) AFPM topology is a type of AFMs consisting of a stator and a rotor with a single air gap. Due to their simple structure, their cost is low. They are preferred for low torque requirements. The magnets in the rotor apply high attraction to the stator core. This irregular pulling force can cause mechanical distortions in the stator. This unbalanced force can cause vibration and noise in the motor. Torque capacities are low compared to double-sided topologies [19].

Double-Stator Single-Rotor (DSSR) motors are also called internal rotor external stator. In this motor topology, unlike the SSDR machine, the rotor is clamped between two stators. In this structure, permanent magnets require more copper as they are balanced with two stators. Having a single-rotor reduces the amount of magnets used. Magnets can be mounted on the surface of the rotor or embedded in the rotor. Being embedded in the rotor protects the magnets better against impact and corrosion.

Since heat is generated in the stator windings, having the stator structure on the edge structures allows the motor to be cooled better. This increases the motor output power [20].

Single-Stator Double-Rotor (SSDR) is a topology consisting of two rotors around the stator. They are also called TORUS type. The fact that the rotor is bilateral is effective in increasing the power density of the motor. Short stator windings reduce copper and iron losses. The presence of the rotors around the stator facilitates the cooling of the motor by showing the fan effect [21].

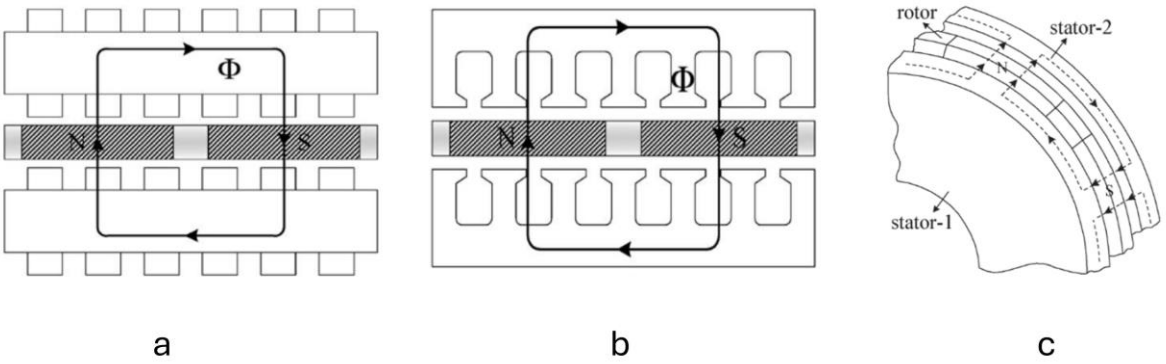

Figure 3. DSSR motor topology a) slotless DSSR b) slotted DSSR c) DSSR motor showing three-dimensional flux paths [22]

Stator structures can be slotted and slotless structures, as shown in the Figure 3. In slotless structures, the windings are wound around the stator core. Winding the windings around the stator causes the end windings to be long [15]. The paths of magnetic flux paths can be NN and NS. In the DSSR NN structure, the magnetic flux leaves the stator, moves circumferentially in the rotor, and returns to the stator. In the DSSR NS structure, the flux from one of the opposite stators passes through the rotor magnets and then to the other stator to complete the flux path. [16].

2.2 Analytical Calculations

AFPMs can be designed according to the requirements of the area of use, required power, and operating conditions. Analytical calculations are made by determining the predictive parameters of the motor to be designed based on efficiency and manufacturability. For the sizing equations, the geometric dimensions of the motor to be designed are determined by first finding the machine output power.

The general sizing equations for AFPMs can be calculated as follows, neglecting leakage resistance and inductance. The output power equation can be found here with the number of phases, phase voltages, and phase currents at a given period with an estimated efficiency [23].

$$P_{out} = \eta \frac{m}{T} \int_0^T e(t).i(t)dt = mK_P \eta E_{pk} I_{pk} \quad (1)$$

The machine efficiency is denoted by η in the above output power P_{out} formula. $e(t)$ is the phase air-gap EMF, $i(t)$ is the phase current, m is the number of machine phases, and T is the period of a single

EMF cycle. Phase air-gap EMF peak value is denoted by E_{pk}, phase current peak value by I_{pk}, electrical power wave factor by K_P, and current wave factor by K_i,. These are described as follows:

$$K_P = \frac{1}{T}\int_0^T \frac{e(t).i(t)}{E_{pk}.I_{pk}}dt \;=\; \frac{1}{T}\int_0^T f_e(t).f_i(t)\,dt \qquad 2$$

$$K_i \;=\; \frac{I_{pk}}{I_{rms}} \;=\; \frac{1}{\sqrt{\frac{1}{T}\int_0^T \left(\frac{i(t)}{I_{pk}}\right)^2 dt}} \qquad 3$$

Where the normalized EMF and current waveform expressions are denoted by $f_e(t) = \frac{e(t)}{E_{pk}}$ and $f_i(t) = \frac{i(t)}{I_{pk}}$. The phase-current rms value is denoted by I_{rms}. The waveform's peak, E_{pk}, is computed as follows:

$$E_{pk} \;=\; K_e N_{ph} B_g \frac{f}{p}(1 - \lambda^2)D_0^2 \quad \lambda = \frac{D_i}{D_o} \qquad 4$$

K_e is the EMF component that includes the winding distribution factor (K_w) and the area of the air gap per unit that is covered by the machine's salient poles, if any; f is the converter frequency; p is the machine pole pairs; B_g is the flux density in the air gap; N_{ph} is the number of turns per phase; and λ diameter ratio is the ratio of the inner surface (D_i) to the outer surface (D_o). The peak phase current is:

$$I_{pk} = \; A\pi K_i \frac{1+\lambda}{2}\,\frac{D_0}{2m_1 N_{ph}} \qquad 5$$

where A is the electrical load and m_1 is the number of phases in each stator. The general output formula can be identified in the following equation when the P_{out} formula from Equation 1 is written to the ones from the Equation 4 and Equation 5.

$$P_{out} \;=\; \frac{m}{m_1}\frac{\pi}{2}K_e K_i K_p \eta B_g A \frac{f}{p}(1-\lambda^2)\left(\frac{1+\lambda}{2}\right)D_0^3 \qquad 6$$

2.3 Multi-Objective Optimization Genetic Algorithm (MOGA)

Optimization in electrical machine design is an important tool for improving performance, efficiency, cost, and other technical requirements. Different optimization methods are used for this purpose. Nonlinear Programming (NLP) offers a suitable approach for design problems with nonlinear costs and constraints [24]. In addition, GA is a method inspired by biological evolutionary processes and is especially preferred for multi-objective optimization problems [25]. Particle Swarm Optimization (PSO), a technique based on ensemble intelligence, achieves efficient results in high-dimensional problem spaces [26]. Response Surface Methodology (RSM) contributes to the design process based on mathematical modeling of design parameters, while machine learning-based methods are increasingly used in modern data-driven design processes [27]. These optimization techniques aim to improve the magnetic, thermal, and mechanical performance of electrical machines while reducing design time and costs.

MOGA, the multi-objective optimization version of GA, offers significant advantages in the design process. Gas were developed as a population-based optimization technique similar to the biological evolution process [28]. Figure 4 shows the flow diagram of MOGA. In this study, magnet optimization is carried out by using FEM in the design of electric motors with simulations made through the ANSYS program. One of the factors that directly affects the performance of electric motors, such as Permanent Magnet Synchronous Motors (PMSM) is the geometrical properties and volumetric parameters of the magnet. [29]. In particular, the effect of the magnet on the torque ripple and average torque value is critical for the efficiency and operability of the motor [30]. In this context, in this study, it is aimed to keep the torque ripple value below 10% and the average torque value above 21 Nm. The MOGA technique was used to optimize the geometrical parameters of the magnet. This optimization method balances multiple objectives, aiming both to minimize the torque ripple and to increase the average torque value to the desired level. As a result, the targeted performance criteria were achieved by optimizing the parameters of the magnet, such as inner diameter, outer diameter, and embrace values.

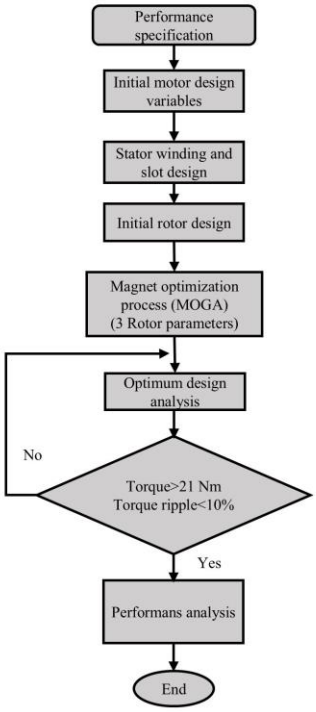

Figure 4. Flow chart of motor design [31]

The optimization process of the study was done by considering the interaction of parameters such as torque ripple and average torque value in motor design. MOGA was used as a powerful method to effectively analyze the effects of design parameters and determine the optimal values of different parameters. In this optimization process, 3 parameters were optimized for 2 target values. For MOGA, the initial sample size, sample size per iteration and maximum iteration size are defined as 100, 50 and 20 respectively. This algorithm was able to optimize both objectives at the same time and increase the average torque value by reducing the torque ripple below the desired limits. As a result, the optimization data obtained allowed the accurate determination of the design parameters required for more efficient and reliable operation of electric motors. Table 1 shows the optimization parameters and their target values.

Table 1. Optimization parameter and target value

Parameter	Calculation range	Condition	Goal
Average torque	0.06s:0.1s	>=	21 Nm
Torque ripple	0.06s:0.1s	<=	0.10

3. Design and Result

3.1 Analytical Design Result

The double-stator single-rotor AFPM motor is particularly notable for its high torque capacity and efficiency advantages. This motor construction provides a more balanced magnetic field thanks to the stators on both sides of the rotor, thus improving the motor's performance. Furthermore, the axial flux structure of the rotor ensures that the magnetic flux is directed parallel to the axis of the motor, resulting in efficient torque generation.

In this study, a 4-pole DS-AFPMSM motor with a shaft power of 3.3 kW was designed. In particular, the advantages of symmetrical torque distribution and high-power density provided by the double-stator structure were taken into account in the motor design. The double-stator structure allows the motor to produce higher torque, while the heating and mechanical loads are more evenly distributed.

The design of the motor was carried out analytically according to the targeted performance parameters. Due to the double-stator construction, the efficiency and torque capacity of the motor are significantly increased compared to single-stator models. This design is optimized to meet particularly high dynamic performance requirements. The analytical calculations of the motor and the obtained performance values are presented in Table 2.

Table 2. Some of the calculated values

Motor Parameters	**Value**	**Unit**
Stator outer diameter	150	mm
Stator inner diameter	80	m
Stator current	5.56	A
Stator’s winding number per phase	26	turns
Back EMF	198	V
Magnet thickness	3	mm
Air gap	0.75	mm
Stator’s winding resistance per phase	2.12	Ω
Output power	3312	W
Input power	3561	W
Efficiency	93	%
Electromagnetic torque	21.09	Nm

3.2. Torque Ripple Optimization with MOGA

In this study, the MOGA optimization method is used to minimize the torque ripple value. ANSYS provides significant convenience to the users in performing the optimization process with the toolkit developed for such applications. In ANSYS software, the optimization process was carried out by making the necessary definitions through the relevant interface. The main objective of this study is to keep the average torque value above 21 Nm and, at the same time, to reduce the torque ripple value to a level below 10%. The optimization process was carried out over three parameters. These

parameters are the embrace value of the magnet and the inner and outer diameter values of the magnet, each of which is defined within certain limits. The limits defined in the study are presented in Table 3.

Table 3. Limit values in magnet optimization

Parametre	Min Value	Max Value
Magnet embrace	0.7	0.99
Magnet inner diameter	80 (mm)	95 (mm)
Magnet outer diameter	125 (mm)	150 (mm)

3.3. Magnetic Design

The magnetic design of the AFPM was performed using ANSYS 2023 R2 software. The advanced simulation capabilities offered by ANSYS provide significant advantages, especially in the analysis of complex magnetic fields and dynamic behavior. However, the 3D modeling of the double-stator AFPM was performed using FEM, which required the implementation of high-resolution mesh structures and took a considerable amount of time. Therefore, in order to save time and computational resources, a one-sided quarter model approach is used, which accurately reflects the behavior of the motor but with a lower resolution. This quadrant model provided the required accuracy in simulating the motor and significantly reduced the solution time. The full magnetic model is presented in Figure 5, and the quarter model is shown in Figure 6. This method provided an efficient balance in the design process and allowed the magnetic properties of the motor to be accurately simulated. The enlarged motor sections shown in Figure 5, where part 1 is the stator and part 2 shows the stator windings. Parts 3 and 4 are magnets and rotor parts, respectively. Table 4 shows the material types used in the analysis of the motor parts.

.

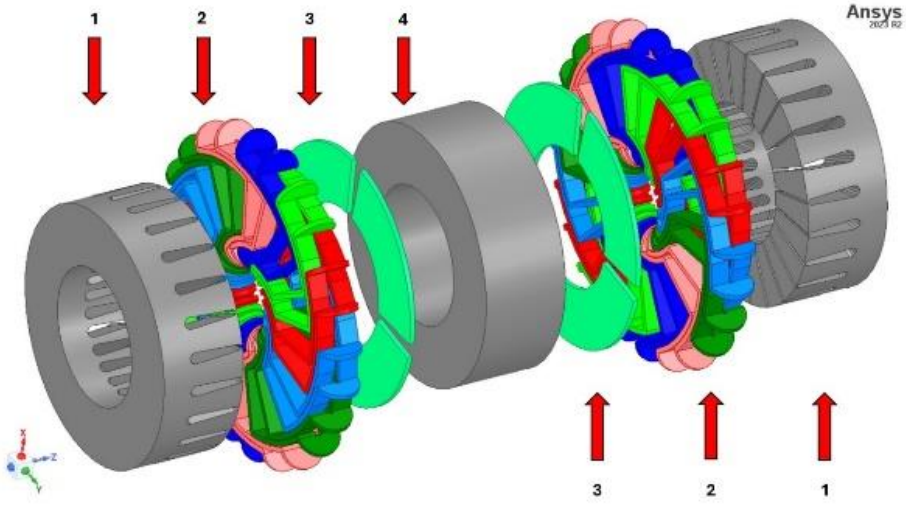

Figure 5. DS-AFPM Motor Full Model (1 Stator core 2 Windings 3 Magnets 4 Rotor core)

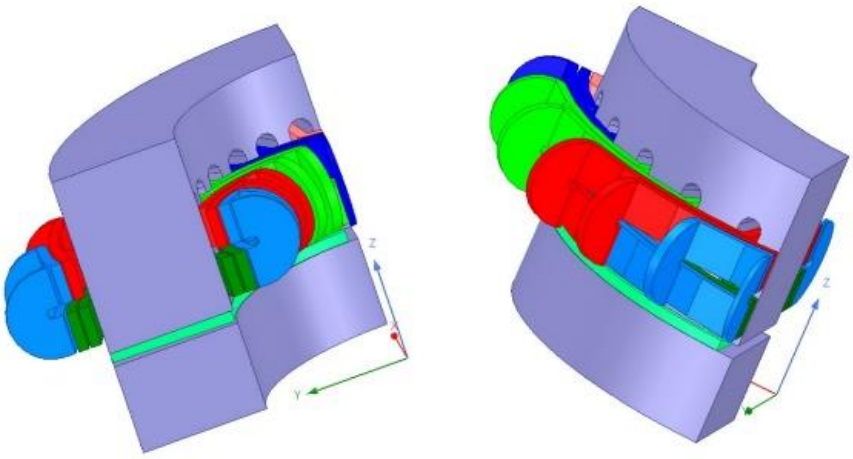

Figure 5 ¼ Model used for FEM

Table 4 Materials used in motor parts

Motor Part	Material
Stator	JFE_Steel_35JN250
Rotor	JFE_Steel_35JN250
Magnet	Arnold_3DSF1000
Windings	copper

During the motor analysis performed in the ANSYS program, the quality of the mesh structure created is of major importance in order to obtain an accurate solution. In this context, the TAU method was preferred as the mesh method. The TAU method is a technique preferred to provide high accuracy, especially in problems with complex geometry. The most important advantage of this method is that it can precisely capture all physical changes in the solution domain. The mesh structure used in the analysis varies with the point densities determined in different regions of the motor. In the stator region, 26684 nodes allow accurate modeling of the detailed flow and magnetic fields in the stator region, while the stator core, rotor core, and magnets have 4215, 4314, and 13047 nodes, respectively. Increasing the mesh density in the airgap region between the rotor and stator allows an accurate simulation of the operating efficiency and electromagnetic behavior of the motor. As a result, this mesh structure, which contains 77404 nodes in total with the nodes in other areas, allows the physical properties of each part of the motor to be modeled with high accuracy and increases the reliability of the solution. The resulting mesh structure is given in Figure 6.

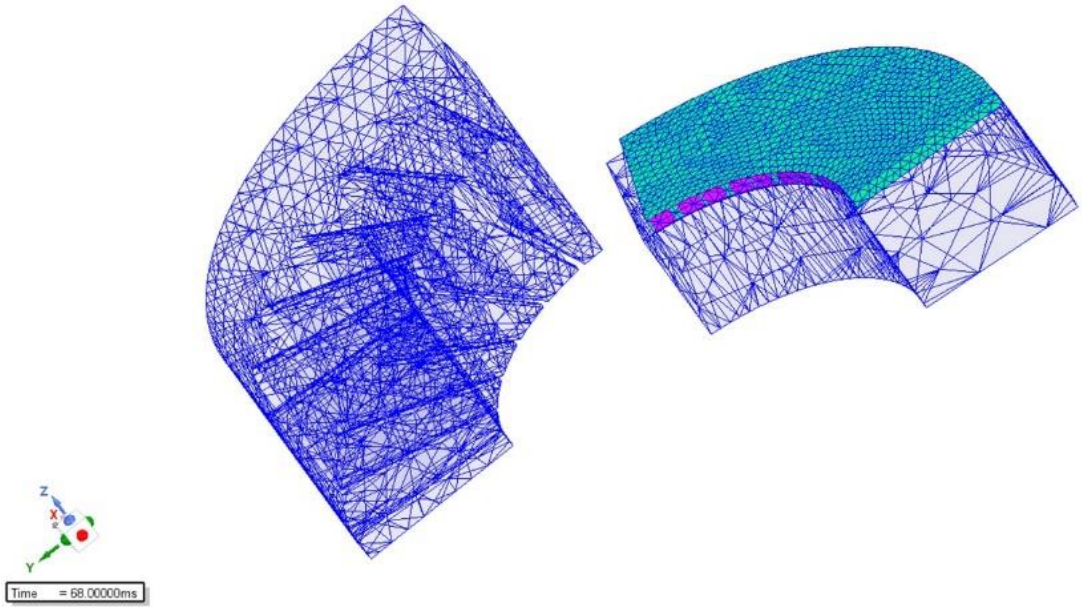

Figure 6. Mesh structure

4. Results

The 3D FEM analysis performed for the DS-AFPM motor allows a detailed study of the dynamic performance of the motor. This analysis was performed over a period of 100 ms with an accuracy of 0.0002 ms each. A 4-pole DS-AFPM with 4 poles and 3.3 kW shaft power was designed and operated under full load (21 Nm). The FEM analysis performed in accordance with the parameters aims to model the electromagnetic behavior, mechanical performance, and electrical efficiency of the motor in more detail.

A 3D solid model of the analytically designed DS-AFPM motor was created, and necessary definitions were made. Although the results obtained from the model analyzed with FEM are generally close to the calculations, the torque ripple value was obtained above the target value. In order to reduce this value, the 3D model of the DS-AFPM motor was analyzed again with the definitions made in Table 5. The average torque and torque ripple values obtained as a result of optimization for different magnet embraces, magnet inner and outer diameters were obtained

According to the results given in Table 5, 3D FEM analysis was performed by entering the motor embrace value 0.917235356, the magnet inner value 80.88125000 mm ; and the magnet outer diameter value 149.5324970 mm.

The data obtained after the FEM analysis allows to examine the variations of various important parameters (three-phase stator current, torque, efficiency, power factor, etc.) that reflect the dynamic performance of the motor with respect to time. Each of these parameters exhibits a specific dynamic behavior depending on the operating conditions of the motor, and this data is critical for the optimization of the motor design. Figure 7 - Figure 9 shows the 3-phase current graphs, torque curve, and induced voltage graphs of the motor.

Table 5. Magnet optimization values

Embrace	Inner Diameter (mm)	Outer Diameter (mm)	Avg Torque (mm)	Torque Ripple (%)
0.700000000	94.25446038	140.0000000	18.35	0.1338
0.700000000	95.00000000	140.0000000	17.92	0.1548
0.710833333	80.62500000	140.4166667	20.40	0.1181
0.723316876	93.15483210	142.8081334	19.62	0.1308
0.724188271	91.47773544	145.1159546	20.17	0.0930
0.732500000	88.12500000	143.7500000	19.98	0.1462
0.743759605	83.79040737	141.8331089	20.56	0.1312
0.754166667	84.37500000	147.0833333	21.27	0.1151
0.755377233	89.53913032	142.0856957	19.83	0.2534
0.775833333	91.87500000	141.5277778	19.03	0.1613
0.792908842	91.07409955	143.8803423	20.59	0.2113
0.797500000	82.50000000	144.8611111	21.26	0.1583
0.810892356	90.58918279	140.3563652	19.34	0.1528
0.819166667	90.00000000	148.1944444	21.35	0.1462
0.837636737	94.20003102	143.1906950	19.77	0.0837
0.840833333	86.25000000	142.6388889	21.10	0.0772
0.855444500	85.14016258	148.3983013	21.53	0.1550
0.862500000	93.75000000	145.9722222	20.71	0.0598
0.867119857	93.71658756	141.0521219	19.33	0.0851
0.883326025	90.28344823	142.4692946	20.25	0.0694
0.884166667	81.56250000	149.3055556	21.87	0.1368
0.905833330	89.06250000	140.7870370	18.59	0.1429
0.905833333	89.06250000	140.7870370	20.07	0.0257
0.917235356	**80.88125000**	**149.5324970**	**21.40**	**0.0738**
0.921055428	92.33201090	143.5786001	20.23	0.0776
0.927500000	85.31250000	144.1203704	20.94	0.1377
0.949166667	92.81250000	147.4537037	20.61	0.1631
0.951021672	92.84639267	141.7366153	19.69	0.1112

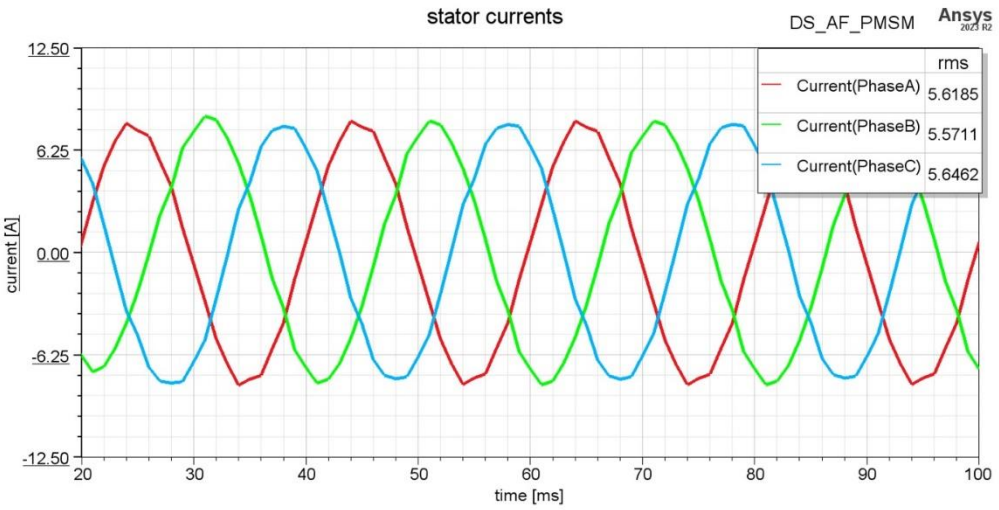

Figure 7. Stator currents at nominal load

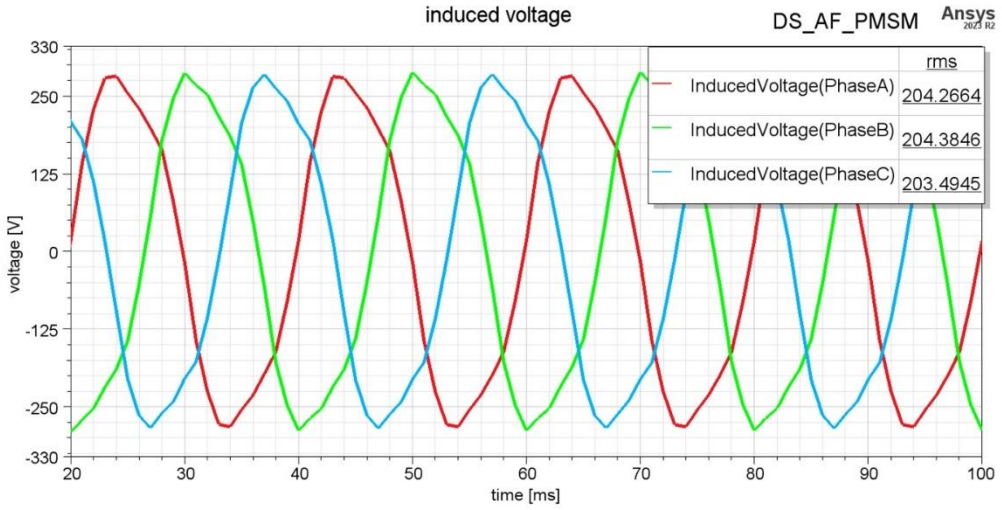

Figure 8. Induced voltage at nominal load

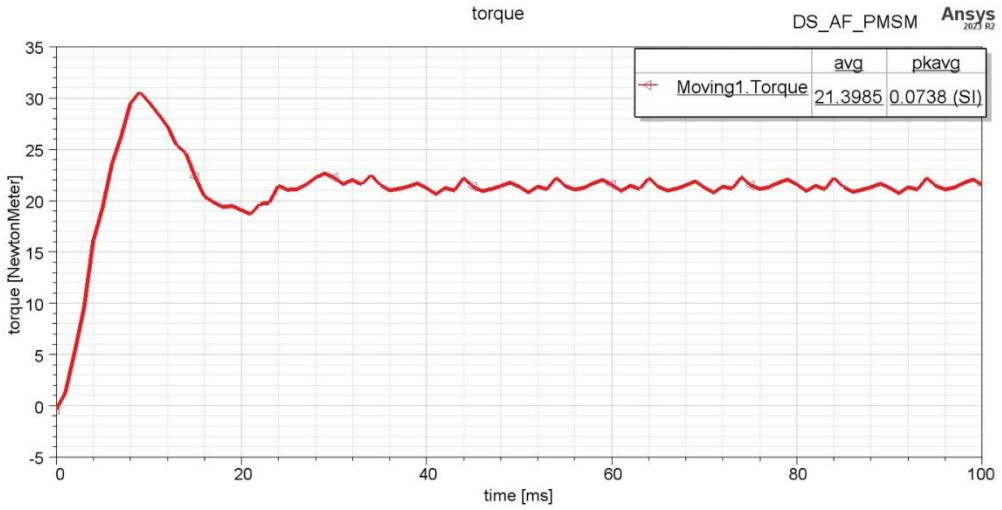

Figure 9. Torque at nominal load

The data obtained for the dynamic performance of the DS-AFPM motor clearly shows that the motor operates in a balanced and efficient mode. As can be seen from the current graph in Figure 7, the three-phase stator currents (Phase A, B, C) exhibit a sinusoidal waveform with respect to time, and each phase matches each other with a phase difference of 120°. This indicates that the motor's supply source provides excellent phase balance and synchronous operation. The rms values of the currents are 5.6185 A (Phase A), 5.5711 A (Phase B), and 5.6462 A (Phase C) respectively. The small differences between these values indicate that the system maintains electrical symmetry and there is no abnormality in the magnetic circuit of the motor. This symmetry of the current waves proves that the motor generates a balanced magnetic field for torque production.

When the induced voltage graph in Figure 8 is examined, it is seen that the voltages generated in each phase also show a sinusoidal structure depending on time. As can be seen from this graph, the RMS values of the induced voltages are 204.2664 V for Phase A, 204.3846 V for Phase B, and 203.4945 V for Phase C, respectively. The differences between these values are very small, which indicates the balance in the magnetic circuit of the motor and the accuracy of the rotor-stator interaction. It is clearly seen that the three-phase voltages vary regularly with a phase difference of 120° to each other. This

phase difference confirms the correct phase matching and synchronous operation of the motor, which is characteristic of synchronous motors. Moreover, this sinusoidal structure shows that the EMF of the motor is induced in an ideal form and the rotor speed is accurately controlled.

The torque graph in Figure 9, which shows the variation of the torque produced by the motor over time, reveals in detail how the motor responds to dynamic load variations. The motor achieved a constant torque value of around 21.3985 Nm on average. It shows that the motor has reached a stable operating condition under load. Also, the small fluctuations observed in the graph show that the motor makes instantaneous corrections to load variations while trying to produce a constant torque. The small difference between peak torque and average torque proves that the dynamic response of the motor is high and the torque loss is minimal even under sudden load changes.

The overall evaluation of these analyses reveals that the DS-AFPM motor operates in a stable and efficient mode, there is no instability in the three-phase currents and voltages, and the motor exhibits a stable performance in dynamic torque production. These data show that the motor is suitable for use in applications requiring high efficiency and is an ideal choice, especially in systems requiring precise control. The results obtained prove that the electromechanical performance of the motor meets the expectations, and the design has been done successfully.

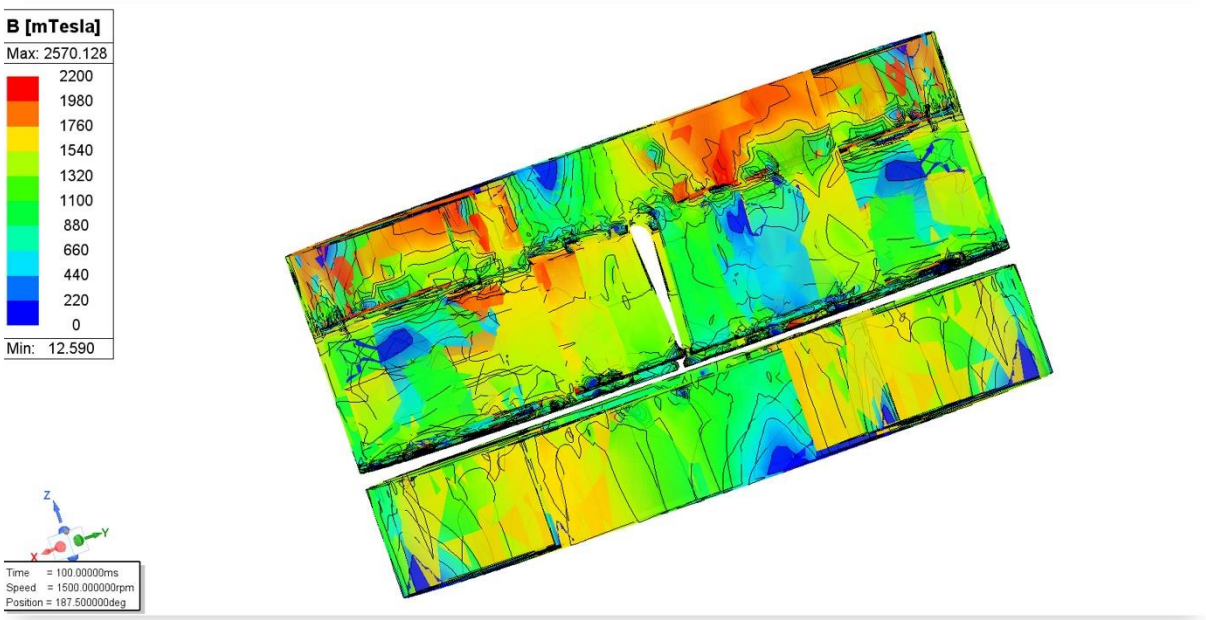

Figure 10. Magnetic flux distribution

In Figure 10, the magnetic flux distribution obtained at the nominal operating conditions of the motor presents the general characteristics of the magnetic field structure of the motor. In the graphs, the maximum value of the magnetic flux density is measured as 2570 mTesla, while the average flux value is between 1500-1700 mTesla. These flux density values show that the densities obtained in various parts of the motor are generally within the reference ranges specified in the literature. Although maximum flux densities are observed at the base of the stator slots and at the end of the slot teeth, the flux densities in the motor are at the desired level.

After obtaining the desired results under nominal operating conditions, the load performance of the designed motor was analyzed. The load analysis was re-analyzed under the same conditions in the

ANSYS program for each load value with 10% load increments from the no-load to 140% load condition of the motor. The results obtained are given in Table 6.

Table 6. Operating values of DS-AFPM motor under different load conditions

Load (%)	Current (A)	Torque (Nm)	Input Power (kW)	Output Power (kW)	Efficiency (%)
10	0.559	2.039	0.336	0.313458	83.11371
20	1.119	4.204	0.678	0.653113	90.27785
30	1.678	6.379	1.027	0.994934	92.45203
40	2.237	8.540	1.381	1.334265	93.26413
50	2.797	10.700	1.740	1.673455	93.53459
60	3.356	12.842	2.104	2.010187	93.52673
70	3.915	14.981	2.473	2.346348	93.36693
80	4.475	17.107	2.847	2.680733	93.10950
90	5.034	19.228	3.224	3.014308	92.78886
100	5.593	21.325	3.605	3.344328	92.41848
110	6.153	23.401	3.989	3.671178	92.01380
120	6.712	25.467	4.377	3.996498	91.58851
130	7.271	27.490	4.767	4.315471	91.13933
140	7.831	29.495	5.159	4.631619	90.67681

As can be seen in Table 6, in the load tests, the motor was loaded up to 40% more than the nominal load in 10 percent increments. In the results obtained, when the motor is operated at values close to the nominal load, it operates with an efficiency higher than 92%, while it operates with an efficiency of 92.41% at the nominal load. The power factor values in the motor operating conditions are generally close to 1.

5. Conclusion

In this paper, DS-AFPM motor design and optimization process is discussed. In the study, torque ripple minimization and average torque optimization were performed using the MOGA method in order to improve the efficiency and performance of the motor. During the design process, the electromagnetic and mechanical performance of the motor was evaluated using analytical calculations and FEM with ANSYS software. It was observed that the motor operates at a shaft power of 3.3 kW, with a torque ripple below 10% and an average torque value above 21 Nm. The results show that the motor provides high efficiency and stable operation.

This study designed the DS-AFPM motor, which offers significant advantages in electric motor design due to its high efficiency and torque capacity. As a result of the optimization with MOGA, the torque ripple value of the motor was reduced by 67.42%, and the average torque value was increased by 5.15% to 21.40. In the analysis results of this model, the average RMS value of DS-AFPM stator currents was obtained as 5.60 A, and the efficiency was 92.41%. FEM analysis shows that the dynamic performance of the motor meets the expectations, and electromechanical balance is achieved. As a result, the designed DS-AFPM motor is considered an ideal option for areas with high efficiency and low energy loss requirements, such as electric vehicles and industrial applications.

6. References

[1] W. Cao, A. A. S. Bukhari, and L. Aarniovuori, "Review of Electrical Motor Drives for Electric Vehicle Applications," *Mehran University Research Journal of Engineering and Technology*, vol. 38, no. 3, pp. 525–540, Dec. 2019, doi: 10.22581/MUET1982.1903.01.

[2] W. Cai, X. Wu, M. Zhou, Y. Liang, and Y. Wang, "Review and Development of Electric Motor Systems and Electric Powertrains for New Energy Vehicles," *Automotive Innovation*, vol. 4, no. 1, pp. 3–22, Dec. 2021, doi: 10.1007/S42154-021-00139-Z/TABLES/10.

[3] A. Hughes and B. Drury, *Electric Motors and Drives: Fundamentals, Types and Applications*. Elsevier, 2019. doi: 10.1016/B978-0-08-102615-1.09989-X.

[4] T. Husain, B. Tekgun, Y. Sozer, and M. Hamdan, "Comparison of axial flux machine performance with different rotor and stator configurations," *2017 IEEE International Electric Machines and Drives Conference, IEMDC 2017*, Aug. 2017, doi: 10.1109/IEMDC.2017.8002354.

[5] A. Mahmoudi, S. Kahourzade, N. A. Rahim, and W. P. Hew, "Design, Analysis, and Prototyping of an Axial-Flux Permanent Magnet Motor Based on Genetic Algorithm and Finite-Element Analysis," *IEEE Trans Magn*, vol. 49, no. 4, pp. 1479–1492, Nov. 2012, doi: 10.1109/TMAG.2012.2228213.

[6] N. Pamuk, "Genetik algoritma optimizasyonu kullanılarak senkron makine tasarımı ve uygunluk parametrelerinin belirlenmesi," *Yenilikçi Mühendislik ve Doğa Bilimleri*, vol. 4, no. 2, pp. 276–288, Jul. 2024, doi: 10.61112/JIENS.1392071.

[7] V. I. Vlachou *et al.*, "Overview on Permanent Magnet Motor Trends and Developments," *Energies 2024, Vol. 17, Page 538*, vol. 17, no. 2, p. 538, Dec. 2024, doi: 10.3390/EN17020538.

[8] L. He, Y. Feng, Y. Zhang, and B. Tong, "Methods for temperature estimation and monitoring of permanent magnet: a technology review and future trends," *Journal of the Brazilian Society of Mechanical Sciences and Engineering*, vol. 46, no. 4, pp. 1–29, Dec. 2024, doi: 10.1007/S40430-024-04723-2/FIGURES/17.

[9] A. Hughes and B. Drury, *Electric Motors and Drives: Fundamentals, Types and Applications*. Elsevier, 2019. doi: 10.1016/B978-0-08-102615-1.09989-X.

[10] Toliyat Hamid A. and Kliman Gerald B., *Handbook of Electric Motors*. 2018. Accessed: Dec. 02, 2024. [Online]. Available: https://www.taylorfrancis.com/books/mono/10.1201/9781420030389/handbook-electric-motors-norm-kopp-gerald-kliman-hamid-toliyat

[11] P. Pillay and R. Krishnan, "Modeling Of Permanent Magnet Motor Drives," *IEEE Transactions on Industrial Electronics*, vol. 35, no. 4, pp. 537–541, 1988, doi: 10.1109/41.9176.

[12] H. Wang and J. Leng, "Summary on development of permanent magnet synchronous motor," *Proceedings of the 30th Chinese Control and Decision Conference, CCDC 2018*, pp. 689–693, Dec. 2018, doi: 10.1109/CCDC.2018.8407219.

[13] L. Shao, R. Navaratne, M. Popescu, and G. Liu, "Design and Construction of Axial-Flux Permanent Magnet Motors for Electric Propulsion Applications-A Review," *IEEE Access*, vol. 9, pp. 158998–159017, 2021, doi: 10.1109/ACCESS.2021.3131000.

[14] Z. Hao, Y. Ma, P. Wang, G. Luo, and Y. Chen, "A Review of Axial-Flux Permanent-Magnet Motors: Topological Structures, Design, Optimization and Control Techniques," *Machines*, vol. 10, no. 12, Dec. 2022, doi: 10.3390/MACHINES10121178.

[15] S. Kahourzade, A. Mahmoudi, H. W. Ping, and M. N. Uddin, "A comprehensive review of axial-flux permanent-magnet machines," *Canadian Journal of Electrical and Computer Engineering*, vol. 37, no. 1, pp. 19–33, 2014, doi: 10.1109/CJECE.2014.2309322.

[16] R. Huang, Z. Song, H. Zhao, and C. Liu, "Overview of Axial-Flux Machines and Modeling Methods," *IEEE Transactions on Transportation Electrification*, vol. 8, no. 2, pp. 2118–2132, 2022, doi: 10.1109/TTE.2022.3144594.

[17] H. Ouldhamrane, J. F. Charpentier, F. Khoucha, A. Zaoui, Y. Achour, and M. Benbouzid, "Optimal Design of Axial Flux Permanent Magnet Motors for Ship RIM-Driven Thruster," *Machines*, vol. 10, no. 10, Oct. 2022, doi: 10.3390/MACHINES10100932.

[18] A. Hemeida, "Electromagnetic and thermal design of axial flux permanent magnet synchronous machines," *Universiteit Gent*, pp. 1–251, 2017, [Online]. Available: http://hdl.handle.net/1854/LU-8527969

[19] M. Aydin, T. Lipo, S. Huang, and T. A. Lipo, "Axial flux permanent magnet disc machines: A review Axial Flux Permanent Magnet Disc Machines: A Review AXIAL FLUX PERMANENT MAGNET DISC MACHINES: A REVIEW," Conf. Record of SPEEDAM, 2004. [Online]. Available: https://www.researchgate.net/publication/228449891

[20] C. Jenkins *et al.*, "Innovations in Axial Flux Permanent Magnet Motor Thermal Management for High Power Density Applications," *IEEE Transactions on Transportation Electrification*, vol. 9, no. 3, pp. 4380–4405, 2023, doi: 10.1109/TTE.2023.3242698.

[21] F. Sahin, A. M. Tuckey, and A. J. A. Vandenput, "Design, development and testing of a high-speed axial-flux permanent-magnet machine," in *Conference Record of the 2001 IEEE Industry Applications Conference. 36th IAS Annual Meeting (Cat. No.01CH37248)*, 2001, pp. 1640–1647 vol.3. doi: 10.1109/IAS.2001.955754.

[22] M. Aydin, S. Huang, and T. A. Lipo, "Torque quality and comparison of internal and external rotor axial flux surface-magnet disc machines," *IEEE Transactions on Industrial Electronics*, vol. 53, no. 3, pp. 822–830, 2006, doi: 10.1109/TIE.2006.874268.

[23] A. Mahmoudi, H. W. Ping, and N. A. Rahim, "A comparison between the TORUS and AFIR axial-flux permanent-magnet machine using finite element analysis," in *2011 IEEE International Electric Machines & Drives Conference (IEMDC)*, 2011, pp. 242–247. doi: 10.1109/IEMDC.2011.5994853.

[24] G. Cornuéjols, J. Pena, and R. Tütüncü, "Nonlinear Programming: Theory and Algorithms," 2018, pp. 305–320. doi: 10.1017/9781107297340.021.

[25] F. Çalişkan, H. Yüksel, M. Dayik, S. Demirel Üniversitesi, A. Meslek Yüksekokulu, and T. Bilimler Meslek Yüksekokulu, "Genetik Algoritmaların Tasarım Sürecinde Kullanılması," *SDU Journal of Technical Science*, vol. 2, no. 6, pp. 21–27, 2016, Accessed: Dec. 03, 2024. [Online]. Available: https://dergipark.org.tr/tr/download/article-file/227734

[26] S. Molaei, H. Moazen, S. Najjar-Ghabel, and L. Farzinvash, "Particle swarm optimization with an enhanced learning strategy and crossover operator," *Knowl Based Syst*, vol. 215, p. 106768, 2021, doi: https://doi.org/10.1016/j.knosys.2021.106768.

[27] Y. Zhang and Y. Wu, "Introducing Machine Learning Models to Response Surface Methodologies," 2021. doi: 10.5772/intechopen.98191.

[28] S. Katoch, S. S. Chauhan, and V. Kumar, "A review on genetic algorithm: past, present, and future," *Multimed Tools Appl*, vol. 80, no. 5, pp. 8091–8126, 2021, doi: 10.1007/s11042-020-10139-6.

[29] J. Liu and Q. Zhou, "Design and Optimization of Permanent Magnet Synchronous Motor Based on Finite Element analysis," in *2019 14th IEEE Conference on Industrial Electronics and Applications (ICIEA)*, 2019, pp. 2055–2058. doi: 10.1109/ICIEA.2019.8834332.

[30] K.-I. Jeong *et al.*, "Magnetic Screen Effects on Torque Ripple and Efficiency of Dual Air-Gap Surface Permanent Magnet Synchronous Motor," *Energies (Basel)*, vol. 16, no. 19, 2023, doi: 10.3390/en16196969.

[31] E. Eser and N. Üstkoyuncu, "Design and Analysis of a Novel Axial Flux Permanent Magnet Assisted Synchronous Reluctance Motor," *Journal of Electrical Engineering & Technology 2024*, pp. 1–10, Oct. 2024, doi: 10.1007/S42835-024-02052-X.